Quaternary Science Reviews 187 (2018) 80–93

Contents lists available at ScienceDirect

Quaternary Science Reviews

journal homepage: www.elsevier.com/locate/quascirev

Middle Holocene marine flooding and human response in the south Yangtze coastal plain, East China

Zhanghua Wang [a, *], David B. Ryves [b], Shao Lei [c], Xiaomei Nian [a], Ye Lv [a], Liang Tang [a], Long Wang [a], Jiehua Wang [c], Jie Chen [d]

[a] State Key Laboratory of Estuarine and Coastal Research, East China Normal University, Shanghai, 200062, China
[b] Centre for Hydrological and Ecosystem Science (CHES), Department of Geography, Loughborough University, Loughborough, LE11 3TU, UK
[c] Ningbo Municipal Institute of Cultural Relics and Archaeology, Ningbo, 315000, China
[d] Shanghai Museum, Shanghai, 200003, China

ARTICLE INFO

Article history:
Received 19 January 2018
Received in revised form
28 February 2018
Accepted 5 March 2018

Keywords:
Palaeo-typhoon event
Sea-level rise
Coastal flooding
Neolithic

ABSTRACT

Coastal flooding catastrophes have affected human societies on coastal plains around the world on several occasions in the past, and are threatening 21st century societies under global warming and sea-level rise. However, the role of coastal flooding in the interruption of the Neolithic Liangzhu culture in the lower Yangtze valley, East China coast has been long contested. In this study, we used a well-dated Neolithic site (the Yushan site) close to the present coastline to demonstrate a marine drowning event at the terminal stage of the Liangzhu culture and discuss its linkage to relative sea-level rise. We analysed sedimentology, chronology, organic elemental composition, diatoms and dinoflagellate cysts for several typical profiles at the Yushan site. The field and sedimentary data provided clear evidence of a palaeo-typhoon event that overwhelmed the Yushan site at ~2560 BCE, which heralded a period of marine inundation and ecological deterioration at the site. We also infer an acceleration in sea-level rise at 2560–2440 BCE from the sedimentary records at Yushan, which explains the widespread signatures of coastal flooding across the south Yangtze coastal plain at that time. The timing of this mid-Holocene coastal flooding coincided with the sudden disappearance of the advanced and widespread Liangzhu culture along the lower Yangtze valley. We infer that extreme events and flooding accompanying accelerated sea-level rise were major causes of vulnerability for prehistoric coastal societies.

© 2018 Elsevier Ltd. All rights reserved.

1. Introduction

Global sea-level rise is predicted to accelerate during the 21st century and could rise 65 ± 12 cm by 2100 compared with 2005 (Kopp et al., 2016; Nerem et al., 2018), which will increase the frequency of extreme events and the risk of coastal flooding (Woodruff et al., 2013). The vulnerability of low-lying coastal plains and deltas across the world is further exacerbated due to human-induced sediment starvation and land sinking (Syvitski et al., 2009; Giosan et al., 2014). The west Pacific Ocean coast is one of the most vulnerable regions in the world because it is characterized by active tropical cyclones (Woodruff et al., 2013) and, in recent decades, its rate of relative sea-level rise is three times higher than the global mean (Nicholls and Cazenave, 2010). In the densely-populated Yangtze delta, East China (Fig. 1), models under future climate scenarios predict an increase in flood risk from extreme events and relative sea-level rise by 150%–400% in the next 50 years (Tessler et al., 2015). In fact, Typhoon Fitow (the strongest October typhoon making landfall in China for over 60 years) in 2013 caused flooding to a depth >0.5 m across most of the Yaojiang Plain, south east of the Hangzhou Bay (Fig. 1C). There is thus clearly an urgent need for integrated research on sea-level rise, extreme events, coastal flooding and human response.

Coastal flooding is not a new threat. The fact that the south Yangtze coastal plains (Fig. 1B) hold relative thick and rich archaeological records, preserved in marine and deltaic flood basin sediments (Zong et al., 2007; Zheng et al., 2012), is direct witness of past flooding of these areas during human occupation. Neolithic people including the well-known Kuahuqiao, Hemudu and Liangzhu cultures settled and practiced flood management on the coastal wetlands of Hangzhou Bay (Fig. 1) since ~6000 BCE (Zhao, 1998; Zong et al., 2007; Liu and Chen, 2012; Qin, 2013; Liu et al.,

* Corresponding author.
E-mail address: zhwang@geo.ecnu.edu.cn (Z. Wang).

https://doi.org/10.1016/j.quascirev.2018.03.001
0277-3791/© 2018 Elsevier Ltd. All rights reserved.

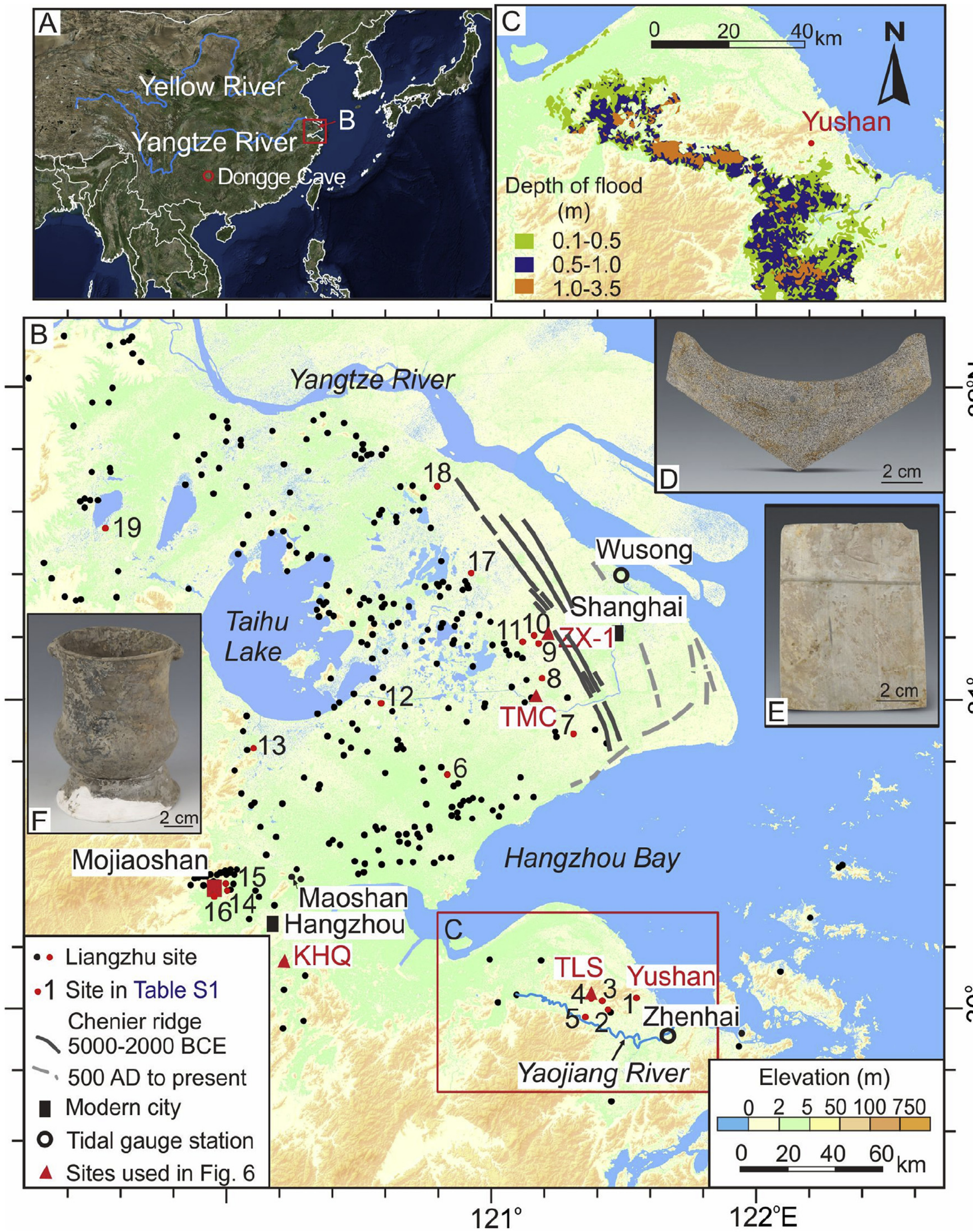

Fig. 1. Location maps. (**A**) East Asia and the location of the study area. (**B**) The south Yangtze coastal plain, showing the locations of the Liangzhu sites and all sites for which radiocarbon dates for the Liangzhu and post-Liangzhu cultural layers were available. These sites are numbered in sequence according to their distance from the Yushan site (Table S1). Note that the Liangzhu settlements are distributed mainly on the Taihu Plain of the southern Yangtze Delta plain and the Yaojiang Plain on the south east bank of Hangzhou Bay. (**C**) The flooding to a depth of >0.5 m across most of the Yaojiang Plain caused by Typhoon Fitow (the strongest typhoon to make landfall in China for over 60 years), October 2013 (data source: Ningbo gauge station, 2013. http://www.nbswz.com.cn/Html/201405/26/11669.html). (**D**–**F**) Typical artefacts of the Liangzhu culture discovered from the Yushan site, now deposited in Ningbo Municipal Institute of Cultural Relics and Archaeology. (**D**) Stone cutter (*Shi Dao*); (**E**) stone woodworking tool (*Youduan Shi Beng*); (**F**) black pottery two-lugged necked jar (*Shuangbi Hu*), with some remains of black slip. The maps were generated with the ArcGis 10.1 software (www.esrichina.com.cn) using the topographic dataset provided by the International Scientific & Technical Data Mirror Site, Computer Network Information Centre, Chinese Academy of Sciences (http://www.gscloud.cn).

2017). People of the Liangzhu culture, which was one of the most developed and complex societies known in prehistory (Lawler, 2009; Liu and Chen, 2012; Qin, 2013), even constructed massive earth-and-stone walls to hold back floods near their capital city, Mojiaoshan, at the head of Hangzhou Bay near present-day Hangzhou (Fig. 1B; Lawler, 2009; Liu and Chen, 2012; Liu et al., 2017). Yet they abandoned their state capital complex at around 2500 BCE, as shown by dating sedimentary profiles from the capital city (Zhang et al., 2015b; Wang et al., 2017), despite their highly developed techniques in agricultural and landscape management (Zhuang et al., 2014; Liu et al., 2017). The subsequent Neolithic Qianshanyang and Guangfulin cultures that appeared at ~2400–1800 BCE were reported to be much less organized and less developed (Shanghai Museum, 2002; ZPICRA and Huzhou Museum, 2014). Studying these archaeological records with a focus on the linkage between flood deposits and cultural interruptions can shed light on the increasing flood risk in this economically important and populous area in the near future.

There has been much speculation and debate surrounding the Liangzhu cultural decline among archaeologists and environmental scientists. Archaeologists speculate that the abandonment of the Liangzhu capital city might have been related to floods because a layer of silt, inferred as flood deposits, was found on top of the late Liangzhu cultural layer in many areas around the capital city (Liu and Chen, 2012). An early environmental study suggested marine inundation played a key role, based on the marine fossil record of core ZX-1 in the eastern Taihu Plain (Stanley et al., 1999), but later work reported no marine flooding at other sites in the Taihu Plain at this time (Zong et al., 2011). Later Innes et al. (2014) suggested a combination of rising local water level and climatic deterioration was the probable cause. We propose that to settle the debate and test these competing hypotheses, it is necessary to carry out an integrated study of relative sea-level change and environmental and human response. It is particularly important to examine directly the event-character of the floodbeds covering the Liangzhu culture layer recovered from archaeological sites.

The Yushan archaeological site was discovered in 2013. It is only 7.3 km from the present coastline (Figs. 1 and 2A). Diagnostic black pottery and tools for woodworking and farming (Fig. 1D–F) of the Liangzhu culture were recovered from this site. The Liangzhu cultural layer was overlain by mud deposits ~0.4–0.5 m thick which did not contain artefacts, hinting at an inundation event at the end of the Liangzhu culture. Yushan may therefore be key to addressing this debate based on a detailed investigation of the stratigraphic records within this site and may provide important evidence on the mechanisms involved in the decline of the Liangzhu culture. In this study we first carried out multiproxy lithological, sedimentological, palaeontological and organic geochemical analyses of well-dated, high-resolution sequences at multiple locations within the Yushan site to examine the nature of flood deposits covering the Liangzhu cultural layer. We then determined the relative sea level change at the end of the Liangzhu culture using sea level indicators, including the basal peat (Shennan et al., 2015) obtained from the Yushan site. We also synthesised existing profiles from both the Taihu Plain and plains along Hangzhou Bay to compare the flood signatures and to discuss the linkage between relative sea-level rise and flood hazards at the late stage of the Neolithic period on the south Yangtze coast, East China. The results help to resolve this debate over the Liangzhu cultural decline and marine flooding and show the sensitivity and vulnerability of prehistorical human societies to extreme events and flooding.

2. The study area and the site

The south Yangtze coastal plain is mainly made up of the Taihu Plain and coastal plains along the Hangzhou Bay, including the Yaojiang Plain, which is located to the south east and is separated by uplands from Hangzhou Bay (Fig. 1B). Sediments deposited in these plains were derived mainly from the Yangtze River during the Holocene, as sediment load from other local rivers is negligible compared to that from the Yangtze River (Liu et al., 2013). The freshwater-dominated Taihu Plain was formed ~6500–6000 years ago when sea level was relatively stable and the Yangtze delta started its progradation (Hori et al., 2001; Wang et al., 2012). However, the rate of shoreline advance was extremely slow between 6500 and 4000 years ago, as indicated by distribution of the chenier ridges in the east part of the plain (Fig. 1B; Yan et al., 1989), caused mainly by a large amount of sediment trapping in the north Yangtze delta plain (Li et al., 2002; Hori et al., 2001) and the decline in the Yangtze sediment supply owing to weakening of the East Asian Summer Monsoon ~6000 years ago (Zhan et al., 2012). Rapid shoreline accretion only occurred over past 2000 years, in concert with an increase in sediment supply from human activity (Hori et al., 2001; Wang et al., 2011). Sediment cores from the south coastal plain of Hangzhou Bay demonstrate that rapid infilling of Hangzhou Bay occurred during the early Holocene (Gao and Collins, 2014; Zhang et al., 2015a). A long period of sedimentary hiatus then occurred during the middle to late Holocene with return to net sedimentation in Hangzhou Bay only in the past 2000 years (Gao and Collins, 2014; Zhang et al., 2015a).

Tide dominates the south Yangtze coast with a mean tidal range of 2.7 m (Chen et al., 1985). The Yaojiang Plain of south east Hangzhou Bay has a smaller mean tidal range of 1.85 m. Uehara et al. (2002) reconstructed the palaeotidal fields in the Yangtze Estuary and the east China marginal sea by including the effect of palaeo-topographic change from sedimentation since the Last Glacial Maximum. The simulated amplitude M_2 tide, which is the most significant component of tide in this region, was 1.0–1.2 m on the coast south to the Hangzhou Bay (including the Yaojiang Plain) and 1.2–1.4 m on the coast of Taihu Plain during the middle Holocene (6 ka; Uehara et al., 2002). It has increased to 1.2–1.6 m in the inner and south part of the Hangzhou Bay at the present day, while remaining at 1.0–1.2 m in the south east part of the Bay. Ground elevation is 0–2 m above present mean sea level (the Yellow Sea datum, MSL_{YSD}) in most of central Taihu Plain and Yaojiang Plain, and 2–5 m in the plains along Hangzhou Bay (Fig. 1B).

The Yushan site is located in the north east of Yaojiang Plain, between the edge of the upland and the floodplain (Fig. 1). The site was excavated by the Ningbo Municipal Institute of Cultural Relics and Archaeology over an area of 4300 m^2 during September 2014 to January 2015. Each excavation unit is 10 m × 10 m in size (Fig. 2A). The archaeological sequence spans from the early/middle Hemudu culture to the Song dynasty, with ten layers numbered top to bottom correlating to distinct lithology, sedimentology and archaeological finds across the site (Table 1). Individual cultural layers are typically 25–50 cm thick, with the whole sequence spanning 1–2.5 m across the site (Fig. 2B and C). The cultural layers onlap the weathered bedrock or hardened mud surfaces in excavation units close to the upland, such as T0410 and T0513. The Holocene base then dips rapidly and is buried below the floodplain (Fig. 2).

Among the 10 layers (Table 1), layers 9, 7, 6 and 3 are composed of organic-rich mud or peat that contain artefacts of prehistoric early and middle Hemudu, late Hemudu and Liangzhu cultures and from the Shang and Zhou dynasty, respectively. Layers 10, 8, 5 and 4 are devoid of any cultural artefacts and are considered to be formed without human disturbance. Note that layer 7 only occurs at the edge of the upland, such as in unit T0410 (Fig. 2C). In addition, an erosional surface is prominent on top of the peat layer 6a in many units, and this peat layer is totally eroded away even in those units close to the upland (Figs. 2 and 3). Together with the erosional

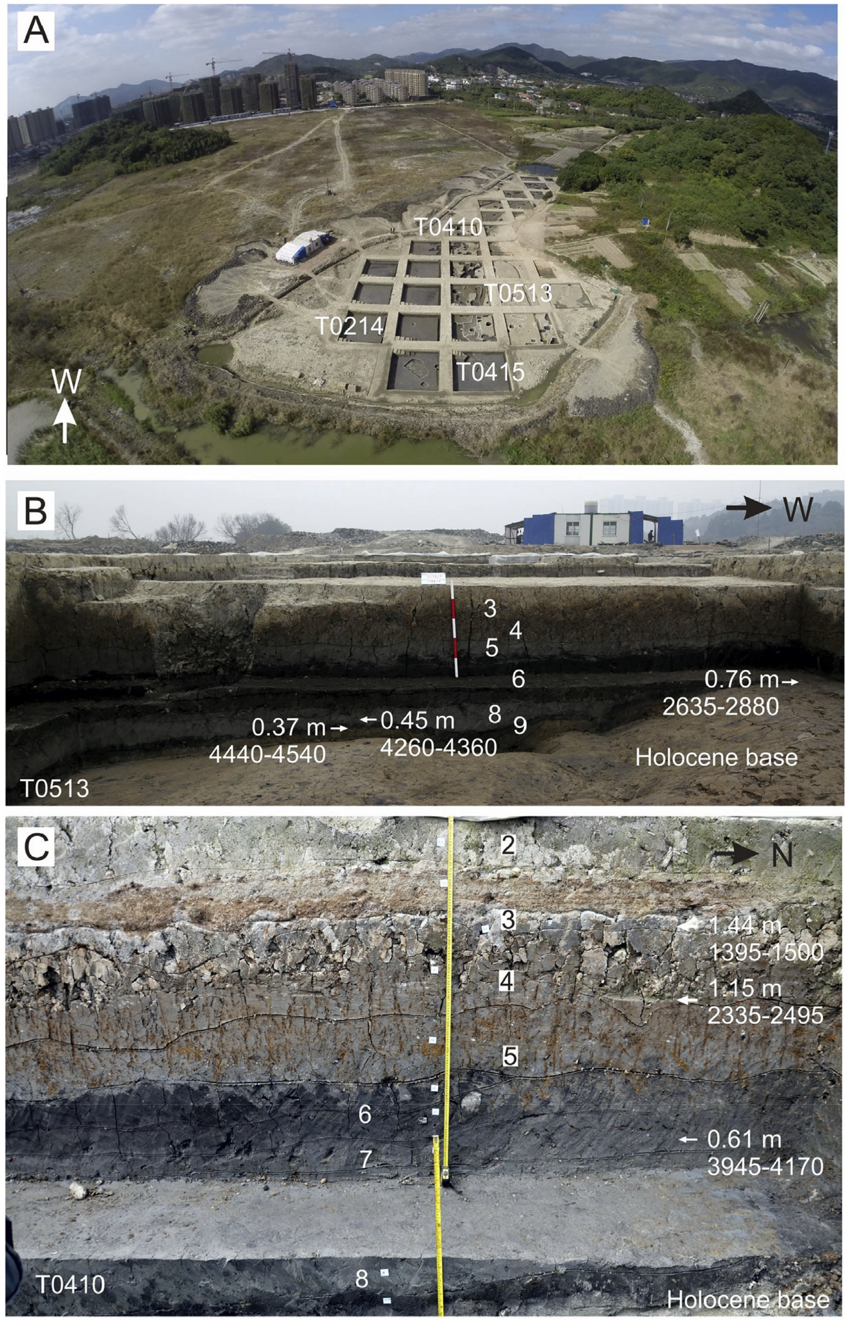

Fig. 2. (**A**). Aerial photo of the Yushan site during excavation. (**B**) Photo of the south wall of unit T0513. Numbers represent the cultural layers. Note layers 8 and 9 pinch out and disappear westward due to the basal topography, making layer 6 the Holocene basal peat in some sections. (**C**) Photo of the west wall of unit T0410. Numbers represent the cultural layers. The data set of altitude and radiocarbon age are presented for each sea-level indicator in (B) and (C). Layers 8 and 9 also pinch out and disappear northward due to the basal topography, making layer 7 the Holocene basal sediments. Elevation of the Holocene bases in two units were measured by a total station. White arrows with elevation and calibrated ages (BCE) represent data used for reconstruction of relative sea level. Numbers of cultural layers: **2**, Tang to Song dynasties; **3**, Shang to Zhou dynasties; **4**–**5**, natural deposits; **6a**–**6b**, Liangzhu period; **7**, late Hemudu period, missing in these units; **8**, natural deposits; **9**, early to middle Hemudu period; **10**, pre-Hemudu natural deposits.

surface, a sand ridge of 20–30 cm high and ca. 60 cm wide that was defined as layer 5b, dips from the edge of upland eastward and cuts into layer 6 (Fig. 3D–F). Gravels, fragments of Liangzhu artefacts and abundant plant fragments were present in the sand ridge. Mixtures of sand and mud, also defined as layer 5b, only occurs above the erosional surface in the area between the sand ridge and the upland.

3. Materials and methods

During our excavation, we carefully examined the lithological and stratigraphic sequences in each excavation unit. We selected the north wall of unit T0415 for analyses of proxies including organic chemistry, diatoms and dinoflagellate cysts, because this unit is on the east edge of the excavation area where less human disturbance occurred (Fig. 2A). We also collected samples for these

Table 1
A summary of the archaeological sequence at Yushan site (Figs. 2 and 3).

Cultural layer	Description of lithology	Archaeological finds	Cultural period
1	Cultivated layer.	None	Present-day
2	Yellowish earth.	Yue Kiln	Tang and Song
3	Dark grey or yellowish grey mud.	Pottery vessels, early proto-celadon, bronze ware, stone and wood tools	Shang and Zhou
4	Yellowish grey mud with some very thin (<1 mm) laminations of silt and abundant root traces.	None	Cultural interruption
5a	Grey homogeneous mud with an unconformity with the underlying layer 6.	None	Cultural interruption
5b	Gravelly sand, sand or mixture of sand and mud.	Some fragments of Liangzhu artefacts.	Storm deposits
6	a, peat; b, peaty mud. On top of this peat layer, an erosional surface occurred and tree stumps exist in many units (Fig. 3A–C).	An artificial platform occurred at the edge of upland, containing pottery vessels, polished stone tools of axe, adze, plow, cutter, arrowhead, sickle and *Mopan* slab. Some artefacts were also found in the peaty mud and peat.	Liangzhu
7	Organic rich mud	Red pottery vessels, polished stone tools of axe, adze, chisel, arrow head and *Mopan* slab and jade.	Late Hemudu
8	Grey homogeneous mud.	None	Cultural interruption
9	Dark grey peaty mud	Black pottery vessels, polished stone tools of axe and adze, bone awl and remains of architecture.	Early to middle Hemudu
10	Yellowish grey or grey homogeneous mud	None	Natural deposition before settling

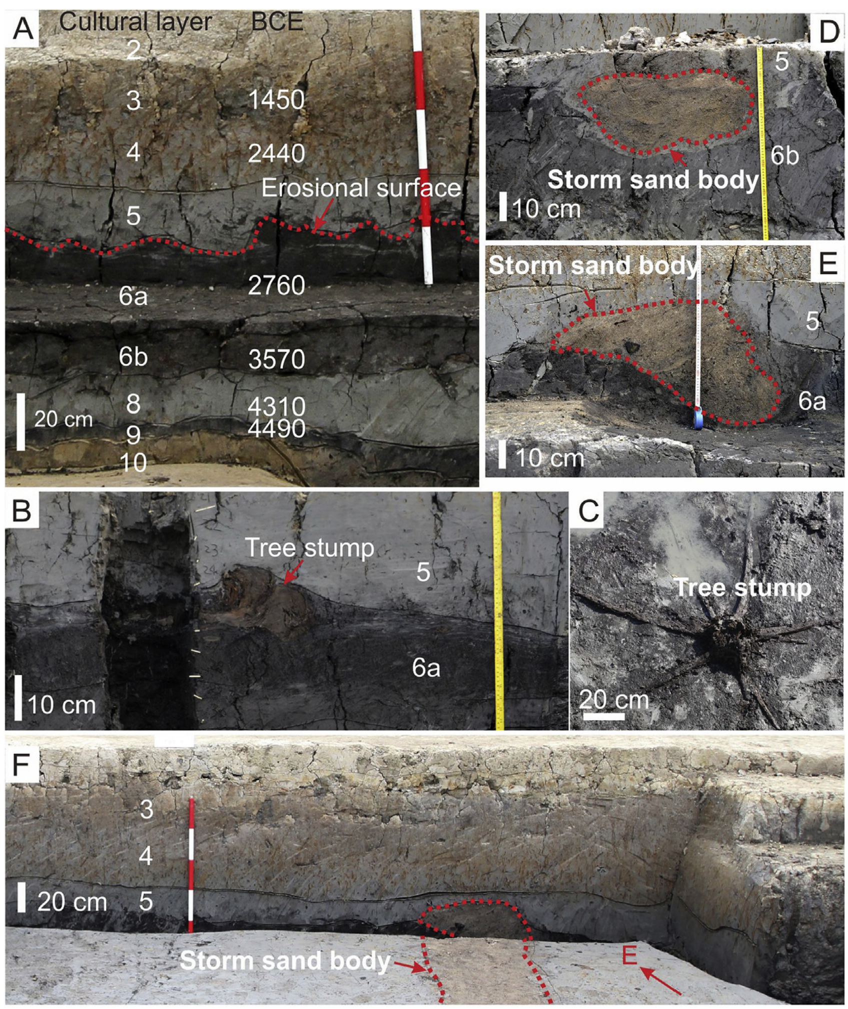

Fig. 3. Photographs of strata at Yushan. (**A**) Excavation unit T0513, showing the sediments deposited since the pre-Hemudu period and the erosional surface above the peat layer of the Liangzhu period. (**B**–**C**) Tree stumps on the tops of the peat layers in T0213 and T0214. (**D**) Sand ridge in T0415. (**E**–**F**) Sand ridge in T0513.

proxy analyses from unit T0410 because layer 7 is missing in unit T0415. We then identified the sedimentary facies of each layer and recognized marine inundation by examining the lithology and analysing proxies.

Twenty-seven (27) samples were collected from the north wall of unit T0415 for analyses of organic carbon and diatoms. Thirty-four (34) samples from layer 3 to 9 from the west wall of unit T0410 and seven samples from layer 6 of unit T0415 were collected for dinoflagellate cyst identification. In addition, seven tree stumps collected from the top of peat layer 6 in units T0214, T0314, T0315 and T0415 were identified at species level at the Institute of Archaeology, Chinese Academy of Social Science.

Samples for organic carbon measurement were dried at 40 °C in an oven and milled to powder. Two aliquots were prepared for each sample: (1) 20 mg powder was used to measure total carbon and total nitrogen (TN) using a vario MAX cube CN analyser (Elementar, Germany) (error <1%) at the State Key Laboratory of Marine Geology, Tongji University, China; (2) about 0.5 g powder was mixed with 0.1 M hydrochloric acid (HCl) for 24 h to remove carbonate and then washed with deionized water thoroughly until the pH was neutral. The neutral specimen was dried at 40 °C and then used for measurement of TOC by vario MAX cube CN analyser (error <1%) at Tongji University and $\delta^{13}C_{V\text{-}PDB}$‰ (error, ±0.2‰; reference material: Urea and Acetanilide) by Delta V Advantage Isotope Ratio Mass Spectrometer (Thermo Scientific, Germany) at the Third Institute of Oceanography, State Oceanic Administration of China. Samples for diatom analysis were prepared at Loughborough University in a water bath using 30% H_2O_2 to remove organic matter and HCl to remove carbonates, following the procedure of Renberg (1990), and permanent slides counted on a Leica DME light microscope (numerical aperture = 1.4) under oil immersion and phase contrast at ×1000 magnification. Samples for dinoflagellate cysts identification were treated following standard procedures of pollen analysis (Moore et al., 1990) and the species were counted using a Leica optical microscope at ×400 magnification. The identification of dinoflagellate cysts was made according to regional taxonomic guides (He et al., 2009; Mao et al., 2011; Tang et al., 2013).

For building the chronology, eight samples of charcoal, plant fragment and organic sediment from units T0410 and T0513 were AMS ^{14}C dated by Beta Analytic, USA, and calibrated using the Calib 7.1 program (Stuiver et al., 2015, Table 2). Furthermore, a sample from the sand ridge above the peat layer in T0513 (Fig. 3E) was dated using single-grain optically stimulated luminescence (OSL) measurement of quartz (Duller, 2008). In total, 3500 grains of quartz (180–224 μm) were measured and 37 grains were accepted for age determination (Table 3; Fig. S1). Luminescence measurements were carried out by an automated Risø-TL/OSL DA-20 DASH reader equipped with a $^{90}Sr/^{90}Y$ beta source (Bøtter-Jensen et al., 2003) and an ET EMD-9107 photomultiplier tube at the State Key Laboratory of Estuarine and Coastal Research, East China Normal University.

We also decided to use the south excavation wall of unit T0513 and west wall of unit T0410 for relative sea level reconstruction. In the south wall of unit T0513, the Holocene base of hardened mud dips gradually from west to east while peaty mud layer 9 and peat layer 6a formed the basal peat from east to west, respectively (Fig. 2B). In the west wall of unit T0410, as the thick layer of peat (layer 6) was eroded away and the sedimentary sequence above the Holocene base is only ~150 cm thick in the north part (Fig. 2C), sediment compaction can be neglected when applying the sea-level indicators from this profile. When collecting the radiocarbon dating material, three sample from layers 9, 8 and 6 in unit T0513, and three samples from layers 7, 4 and 3 in unit T0410 were chosen for reconstruction of relative sea levels (Fig. 2B and C; Table 4). We used the basal peat and stratigraphic approach to determine the palaeo-relative sea levels after identification of these sea-level indicators (Wang et al., 2013; Shennan et al., 2015). We used a total station to measure the elevation of the Holocene base in units T0410 and T0513, where samples of sea-level indicators were collected. We further used the tidal levels calculated from the records of Zhenhai gauge station (Fig. 1B) during AD 1958–1980 because a previous study simulated little change in the tidal range for the coast of Yaojiang Plain from the middle Holocene (6 ka) to the present day (Uehara et al., 2002). As a present-day, high-resolution topographic dataset (http://www.gscloud.cn) demonstrates that the present-day freshwater marsh mostly develops at ~0–0.5 m above the mean spring high water (MSHW) in the Yaojiang plain, freshwater marsh habitat inferred from palaeodata was therefore considered to be 0–0.5 m above the MSHW (Table 4).

In addition, we collected and recalibrated 80 published radiocarbon ages (Table S1) during and after the Liangzhu culture from Neolithic sites across the East China coastal plain using the Calib 7.1 programme (Stuiver et al., 2015) to revise the time span of the Liangzhu culture. We also compiled all published sedimentary profiles dated by AMS ^{14}C in the study area (Fig. S2 for their location) and compared the database covering the end of the Liangzhu culture which included radiocarbon ages (also recalibrated; Table S2), ecological and environmental proxies, and signals of flooding (Table 5).

4. Results

4.1. Holocene stratigraphy and sedimentary environmental change at Yushan

There is clear variation in organic geochemistry in each layer, distinguishing the terrestrial or marine source of organic carbon (Fig. 4). Diatom preservation is poor throughout much of the sequence, and identifiable valves were only observed in layers 9, 8 and 6, and in a single sample of layer 5. Such preservation problems

Table 2
AMS ^{14}C ages and their calibrations for the Yushan and Tianluoshan sites.

Field number	Cultural period	Cultural layer (Fig. 3)	Dating material	$\delta^{13}C$	Conventional age	Calibrated age (BCE)			Laboratory Number
				(‰)	aBP	2 sigma	Probability	Median	
T0410-3c	Shang	3	Charcoal	−25.2	3170 ± 30	1395–1500	1	1450	414776
T0410-4	None	4	Plant fragments	−27.9	3940 ± 30	2335–2495	0.90	2440	414777
T0513-5[a]	None	5	Plant fragments	−25.5	4170 ± 30	2635–2880	1	2760	406454
T0513-6a	Liangzhu	6a	Plant fragments	−30.3	4170 ± 30	2635–2880	1	2760	406455
T0410-6b	Liangzhu	6b	Organic sediments	−27.6	4770 ± 30	3515–3640	0.98	3570	414778
T0410-7	Late Hemudu	7a	Charcoal	−25.6	5210 ± 50	3945–4170	0.94	4020	414779
T0513-8-1	None	8	Plant fragments	NA	5470 ± 30	4260–4360	1	4310	406456
T0513-9	Early to mid- Hemudu	9	Charcoal	−26.3	5640 ± 30	4440–4540	0.83	4490	406457
Tianluoshan[b]	End of the Neolithic	–	Seeds	NA	4020 ± 40	2465–2635	0.98	2540	BA091045
Tianluoshan[‡]	End of the Neolithic	–	Seeds	NA	4015 ± 45	2455–2675	0.97	2540	BA07761

[a] This sample was collected from the sand ridge.
[b] ,‡ Ages for Tianluoshan were obtained from Zheng et al. (2009; 2012) and recalibrated using the Calib 7.1 program, as were other ages in the present study.

Table 3
Single-grain OSL age for the sand ridge sample from the Yushan site together with supporting dose rate and equivalent dose (D_e) data.

Lab No.	U (ppm)	Th (ppm)	K (%)	Water content (%)	Environmental dose rate[a] (Gy/ka)				Over-dispersion	D_e[b] (Gy)	Age ka	Calibrated calendar age (BCE)
					Beta	Gamma	Cosmic-ray	Total				
L144	3.5 ± 0.13	16.3 ± 0.39	2.01 ± 0.06	19 ± 5	1.77 ± 0.10	1.36 ± 0.07	0.18 ± 0.12	3.31 ± 0.12	0.18 ± 0.03	15.2 ± 0.57	4.59 ± 0.24	2575 ± 240[c]

[a] The dose rate and OSL ages were calculated using the 'DRAC' (Durcan et al., 2015).
[b] Single grains of quartz were measured in the regenerative-dose protocol, using a test-dose of 3.03 Gy, a preheat of 200 °C for 10 s, a 160 °C cut heat for 0 s, and green-laser stimulation at 125 °C for 0.9 s. The first 0.06 s of stimulation minus a background estimated from the integral of the last 0.1 s was used for single grain D_e calculation.
[c] This calibrated calendar age was calculated by subtracting 2015 that is the sampling year of the sand ridge from the OSL-dated age 4.59 ± 0.24 ka.

Table 4
Reconstruction of relative sea levels using sea-level indicators obtains from units T0410 and T0513 (Fig. 2B and C). Sedimentary facies was determined according to the lithology, organic carbon, diatoms and dinoflagellate cysts. Tidal levels were collected from the Zhenhai gauge station (Fig. 1; 1958–1980). MSHW, 1.61 m; MHW, 1.17 m; MNHW, 0.63 m. All heights are given with respect to current mean sea level (Yellow Sea datum). Abbreviations: MSHW, mean spring high water; MHW, mean high water; MNHW, mean neap high water.

Unit	Alt. (m)	Cultural layer	Sedimentary facies	Calibrated age (BCE)	Indicative meaning	Palaeo-sea level (m)	Error (m)
T0410	1.44	3	Saltmarsh	1395–1500	MHW–MSHW	0.05	0.22
T0410	1.15	4	Upper tidal flat	2335–2495	MNHW–MHW	0.25	0.27
T0513	1.16[b]	6	Freshwater/brackish marsh	2560[a]	0–0.5 m above MSHW	−0.70	0.25
T0513	0.76	6	Freshwater marsh	2635–2880	0–0.5 m above MSHW	−1.10	0.25
T0410	0.61	7	Saltmarsh	3945–4170	MHW–MSHW	−0.78	0.22
T0513	0.45	8	Upper tidal flat	4260–4360	MNHW–MHW	−0.45	0.27
T0513	0.37	9	Freshwater marsh	4440–4540	0–0.5 m above MSHW	−1.49	0.25

[a] This is the interpolated age, i.e., the age of storm event that drowned the peat layer.
[b] Calibrated value of the original peat top assuming that the peat layer above Holocene base in the west part of T0513 was ~30-cm thick, and had been compacted from an original ~40-cm thick layer, using the highest estimation of percentage (30%) of peat compaction with an overburden of 1 m (van Asselen et al., 2011).

are typical for coastal sediments (Ryves et al., 2004). By contrast, dinoflagellate cysts of marine genera including *Spiniferites*, *Operculodinium* and *Lingulodinium* were found in the non-cultural layers of 8, 5 and 4 and the bottom section of layer 3. Below we present the results of chronology, stratigraphic patterns of proxies and interpretation of sedimentary environments of layers 10–2.

4.1.1. *Layer 10 (mud before the early Hemudu culture)*

Levels of TOC and TN are generally low (<1% and <0.2%, respectively; Fig. 4A) and values of TOC/TN and $\delta^{13}C$ indicate that the dominant source of organic carbon was freshwater algae or freshwater particulate organic carbon (POC) (Fig. 4B; Lamb et al., 2006). A terrigenous environment is thus inferred for the Yushan site before the settlement of Hemudu people.

4.1.2. *Layer 9 (early to middle Hemudu culture)*

A charcoal sample from this peaty mud layer was dated to 4440–4540 BCE (median age 4490 BCE; Table 2), which is in agreement with the artefacts of early to middle Hemudu culture found in this layer. TOC increases to ~5%; $\delta^{13}C$ analyses indicate that the organic carbon was derived from terrestrial C_3 plants and freshwater POC or algae (Fig. 4A and B). Diatoms are sparse in the bottom samples of this layer, consisting of robust, freshwater benthic forms. The middle sample in this section contained several whole cells of *Amphora copulata,* a benthic species more typical of higher conductivity freshwaters. The presence of whole cells suggests that the diatoms were growing *in situ*, rather than transported to the site, implying shallow water. Subsequent samples at the top of this layer 9 included taxa typical of somewhat fresher, low nutrient and lower pH waters, such as *Eunotia* and *Pinnularia*, along with some elongate *Fragilaria*. No marine dinoflagellate cysts was observed. A coastal freshwater marsh environment was identified during the early to middle Hemudu period.

4.1.3. *Layer 8 (artefact-absent mud covering the early to mid-Hemudu cultural layer)*

A radiocarbon age of 4310 BCE (4260–4360 BCE) was obtained from a sample of plant fragments in the bottom section of this layer. TOC decreases sharply (<1%) and its isotopic composition demonstrates a terrestrial origin (Fig. 4B). However, a few valves of marine coastal taxa (such as *Rhaphoneis*) were encountered (Fig. 4A). Furthermore, of the four samples analysed, the uppermost sample had no marine dinoflagellate cysts, while concentrations for the other three were 332, 78 and 365 cysts g^{-1} dry weight (dw). An upper tidal flat environment was thus inferred at the site after the end of the middle Hemudu culture.

4.1.4. *Layer 7 (late Hemudu culture)*

Radiocarbon dating of charcoal from this organic-rich mud layer gives an age of 4020 BCE (3945–4170 BCE; Table 2), supporting the finds of artefacts of late Hemudu culture found in this layer. Organic carbon was derived from freshwater algae or POC and some terrestrial C_3 plants (Fig. 4B). Only two samples contained marine dinoflagellate cysts among five samples in layer 7, with concentrations of 53 and 582 cysts g^{-1} dw. These data indicate a saltmarsh environment during the late Hemudu culture.

4.1.5. *Layer 6 (Liangzhu culture)*

Radiocarbon ages from two samples from the bottom and upper section of this layer are 3570 BCE (3515–3640 BCE) and 2760 BCE (2635–2880 BCE), respectively (Table 2; Fig. 3A), which is consistent with the Liangzhu artefacts found in this layer. Rooted *in situ* at the top of this peat layer are many tree stumps at the edge of the excavation area (Fig. 3B and C), all of which have been identified as mature willow (*Salix*; ~12–25 cm in diameter; 1–6 trees per excavation unit of 100 m^2). This shrub is typical of the natural Yangtze coastal freshwater marsh, a zone located above MSHW (Zong et al., 2007, 2011). Both TOC and TN increase steadily throughout layer 6, reaching values of almost 21% (TOC) and 1% (TN). Values of $\delta^{13}C$ of approximately −28‰ and TOC/TN > 15 imply

Table 5
Sediment profiles with high-resolution AMS ^{14}C ages from the Taihu and Yaojiang Plains and head of the Hangzhou Bay, East China coast. Locations of these profiles are indicated in Fig. S2.

No. (Fig. 1)	Name of site	Dated period (BCE unless stated as AD)	Number of dates from 2000 to 3000 BCE	Covering the end of Liangzhu culture (Y/N)	Ecological and environmental indicators at the end of Liangzhu culture (Y/N)	Proxy	Signal of flooding	Data source
1	Yushan	1450–4490	4 + 1 (OSL)	Y	Y (sedimentation rate:0.5–4 mm yr^{-1})	Lithology, sedimentology, organic geochemistry, diatom, macroflora	Storm and marine flooding	Present study
2	Tianluoshan (TLS)	0–5080	2	Y	Y	Diatom, phytoliths, macroflora	Marine flooding	Zheng et al., 2016
3	Kuahuqiao (KHQ)	1160–9020	1	Y	Y	Lithology	Marine flooding	ZPICRA, 2004
4	Tangmiaocun (TMC)[a]	2730–4020	1	Y	Y	Diatom, rice phytoliths	Slight increase in salinity	Zong et al., 2011
5	ZX-1	685–6650	1	Y	Y	Pollen, foraminifera	Marine flooding	Stanley et al., 1999; Chen et al., 2005
6	Pingwang	860–5225	0	Y	Limited data due to very low sedimentation rate (0.1 mm yr^{-1})	Pollen	Increase in local water level	Innes et al., 2014
7	Luojiang/ Hemudu	AD 955–8155	2	Y	Hiatus inferred from the radiocarbon age (sedimentation rate: 0.1 mm yr^{-1})	Pollen	–	Qin et al., 2011
8	Wujiangbang	5435–6145	0	N	N	Pollen	–	Qin et al., 2011
9	Qingpu	AD 170–3710	1	Y	Y	Pollen	Increase in local water level[b]	Itzstein-Davey et al., 2007
10	Guangfulin[c]	AD 860–4360	1	Y	Y	Pollen	Increase in local water level[d] and increase in saline biota (Chenopodiaceae)	Chen, 2002; Atahan et al., 2008; Wang et al., 2012
11	Siqian	4290–6160	0	N	N	Diatom	–	Zong et al., 2011
12	Tinglin	4640–6250	0	N	N	Diatom, rice phytoliths	–	Zong et al., 2011
13	Longnan	2860–3580	1	Y	Y	Pollen	Increase in local water level	Zong et al., 2012
14	Yuanjiadi	1920–4430	0	Y	Y	Pollen	Increase in local water level	Zong et al., 2012
15	Guoyuancun	1770–1850	0	N	N	Pollen	–	Zong et al., 2012
16	Tianyilu	390–2080	0	N	N	Pollen	–	Zong et al., 2012
17	Caoxieshan	1180–2790	1	Y	Y	Pollen	Increase in local water level[e]	Zong et al., 2012
18	Chuodun	10–1440	0	N	N	Pollen	–	Zong et al., 2012
19	Liangzhu	1120–5605	0	Uncertain due to no age constrain	Y	Pollen	Increase in saline biota (Chenopodiaceae)	Li et al., 2010

[a] The name “Tangcunmiao” in the original paper should be “Tangmiaocun”.
[b] Age-depth model determined by excluding results from old carbon. Increase in local water level is inferred from the increase in abundance of *Typha* and *Triglochin-Potamogeton* type and a decrease in *Artemisia*.
[c] There are two profiles at this site, one from Atahan et al. (2008) and the other (profile-1999) from Chen (2002).
[d] Age-depth model of profile in Atahan et al. (2008) was determined by excluding results from old carbon (Wang et al., 2012). Increase in local water level is inferred from the increase in *Typha* abundance in both profiles. Increase in saline biota (Chenopodiaceae) abundance is seen in profile-1999 by Chen (2002).
[e] End of Liangzhu period is inferred from the abrupt decline in abundance of cultural NPPs at 0.6 m (their Fig. 6a in Zong et al., 2012). Increase in local water level is inferred from the increase in abundance of open freshwater NPPs.

that this OC was dominantly derived from terrestrial C_3 plants. Furthermore, a diverse flora of diatoms typical of shallow, freshwater/slightly brackish conditions appeared, including species of *Cymbella*, *Amphora*, *Gyrosigma*, *Nitzschia* and *Navicula*. Higher up the sequence, taxa typical of more distinctly brackish conditions were also found, including *Ctenophora pulchella*, *Rhopalodia gibba* and *Chaetoceros* cysts, as well as more clearly freshwater and low alkalinity taxa (*Eunotia*, *Pinnularia*, *Cocconeis*), suggesting a mixture of shallow wetland, freshwater and coastal marine habitats in the vicinity of the site. No marine dinoflagellate cysts was found. A coastal freshwater marsh close to the MSHW is inferred during the Liangzhu culture.

4.1.6. Layer 5b (gravelly sand, sand or sand-mud mixture cutting into the Liangzhu peat)

The sedimentary composition of the sand ridge consisting of gravel, sand and fragments of the Liangzhu artefacts indicates strong hydrodynamic force during its formation. A radiocarbon age of 2760 BCE was derived from the plant fragments within the sand ridge, being identical with that of the underlying peat (Table 2), reflecting reworking from the peat. This sand ridge cutting into the peat layer, together with the sedimentary architecture including the erosional surface and tree stumps at the top of the underlying peat layer, reflect strong erosion and sudden deposition during a major storm event. Previous studies has reported similar deposition facies and sequences during storm events, such as the development of chenier ridges on the tidal flat of the Yangtze coast (Yan et al., 1989). OSL dating of single quartz grains within the sand ridge yielded an age of 4.59 ± 0.24 ka BP (with a central age of 2575 BCE; Table 3).

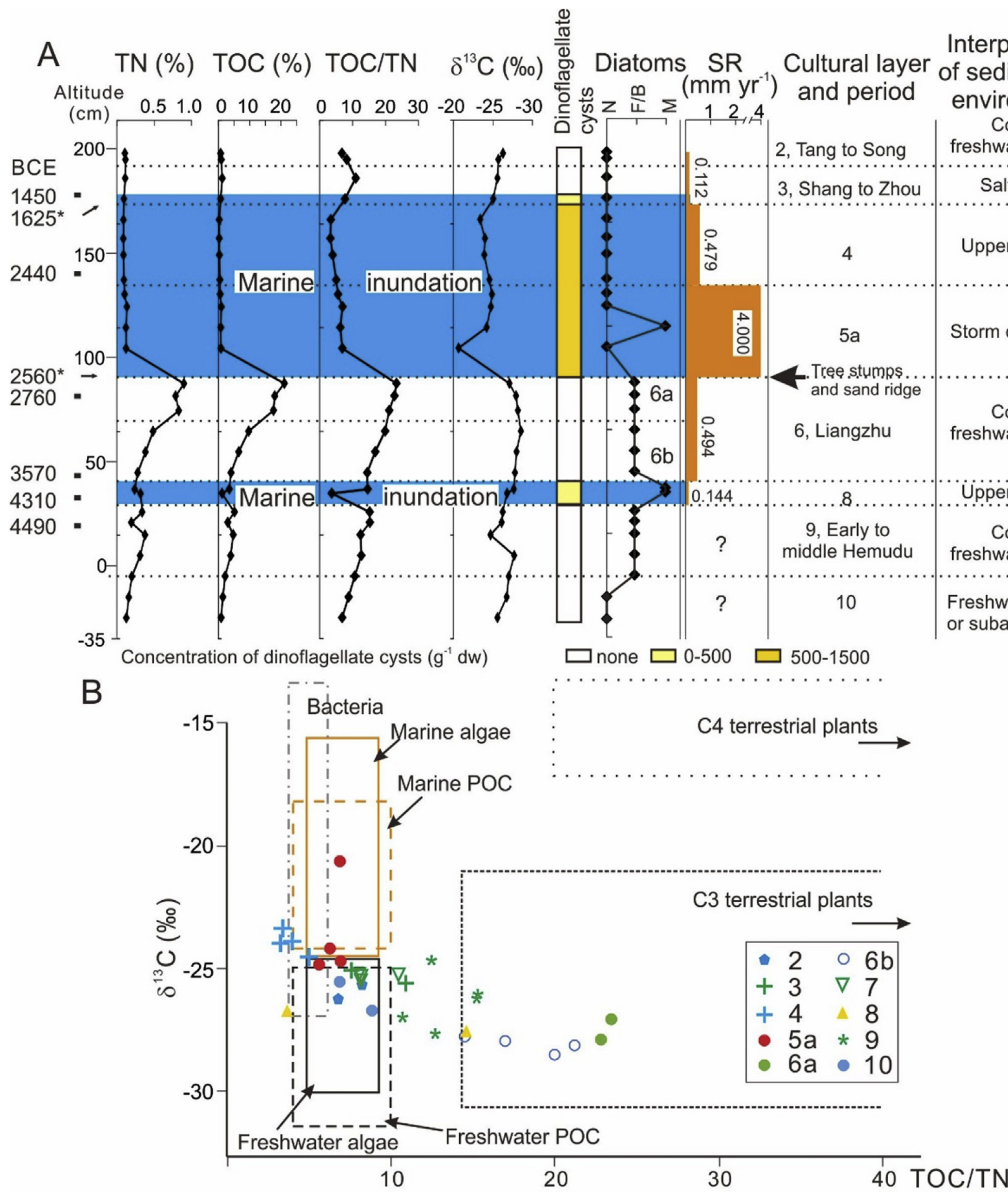

Fig. 4. Environmental change and human responses at Yushan. (**A**) Stratigraphic patterns of total nitrogen (TN), total organic carbon (TOC), TOC/TN, bulk organic carbon stable isotopic composition ($\delta^{13}C$), dinoflagellate cysts, diatoms (N = none, F/B = freshwater/brackish; M = marine; detailed information in Table S4) and sedimentation rates (SR) in different cultural layers (2–10). The numbers used for the cultural layers are the same as in Fig. 3. Ages with stars (*) were calculated based on sedimentation rates. (**B**) Discrimination of organic carbon sources based on TOC/TN and $\delta^{13}C$ (adapted from Lamb et al., 2006).

4.1.7. Layer 5a (artefact-absent mud covering the Liangzhu layer)

Similar to layer 8 which overlies the early to mid-Hemudu peat, layer 5a of homogenous mud overlays the Liangzhu peat in many units. At the bottom of this layer, TOC also abruptly declines to <1% similar to the change from layer 9 to layer 8, with a simultaneous dramatic increase in $\delta^{13}C$ (to −20.66‰) and a decrease in TOC/TN to <8 (Fig. 4A), implying that this organic matter was derived from marine algae or marine POC (Fig. 4B). In the upper part of layer 5, TOC increases slightly and $\delta^{13}C$ shifts to the freshwater algal or POC range, indicating a short period of desalinisation. Some valve fragments of marine plankton (such as large *Coscinodiscus*) were encountered in one sample. Concentration of marine dinoflagellate cysts were abundant (~700–1500 g^{-1} dw) in the whole section. Coastal marine sediment is thus inferred for this layer. We argue that this layer also represents the deposits of the storm event, due to its very high sedimentation rate compared to other layers, and the desalinisation signal inferred from the organic carbon source in the upper part (Fig. 4A). We suggest this mud layer was formed by rapid settling of suspended sediments after the storm, which reworked fine-grained sediments from offshore areas and transported these onshore. The increase in terrestrial organic carbon input in the upper section is an indication of the large amount input of freshwater discharge caused by intense precipitation associated with the storm.

4.1.8. Layer 4 (artefact-absent mud)

An age of 2335–2495 BCE was derived from the bottom of this layer. TOC drops further and was dominated by marine POC or bacterial OC (Fig. 4). Some unidentifiable girdle bands of a large centric diatom, probably a marine planktonic species, was found in one sample. Concentration of marine dinoflagellate cysts is high (500–1500 g^{-1} dw). Together with the lithological feature of silt lamination, we suggest an upper tidal-flat environment during the formation period of layer 4.

4.1.9. Layers 3 (Shang to Zhou dynasty) and 2 (Tang to Song dynasty)

The radiocarbon age of charcoal is 1395–1500 BCE at the bottom of this section, which together with artefacts of Shang to Song dynasties, provides firm evidence that these two layers were formed during the historical period. TOC/TN increased in layers 3 and 2, and OC is dominated by freshwater algae and the POC contains a signal of terrestrial C_3 plants (Fig. 4B). There are some marine dinoflagellate cysts (476 cysts g^{-1} dw) in the base of layer 3, indicating a saltmarsh environment at the beginning of Shang dynasty and a freshwater environment thereafter.

From the results of these multiproxy analyses of organic carbon sources, marine microfossils and the occurrence of human cultural layers, we speculate that humans settled at the Yushan site during periods when coastal freshwater marsh or saltmarsh environment prevailed over the last ~6500 years. However, such settlement was interrupted by two marine intrusion events, corresponding to the interruption of the Hemudu and termination of the Liangzhu culture during ~4310–4020 BCE and 2575–1450 BCE, respectively. Note that the later event was characterized by a major storm event at its beginning, a storm that was strong enough to erode away the peat layer and form a sand ridge.

4.2. Ages of the storm event and the terminal of Liangzhu culture

The OSL dating of quartz grains gives a direct age of 2575 ± 240 BCE for the sand ridge. However, a narrower age span is necessary to discuss the linkage between coastal flooding and the Neolithic culture. As the top of the peat unit at Yushan was eroded away by the storm in many units (Figs. 2 and 3) or possibly lost due to human land use such as building an artificial platform (Table 1), we are unable to determine directly the age when the coastal marsh was inundated and buried by the marine sediments. We therefore compared the ages obtained from the rice field profiles at the Tianluoshan (TLS) site, which is only ~20 km away from Yushan and is located inland and surrounded by highland (Fig. 1B). At the TLS site, the top of the corresponding peat bed formed during the Liangzhu period is non-erosively preserved and dateable (Zheng et al., 2012). This implies that this site was protected from the storm erosion and only drowned by the sea water. Thus, the buried peat top should represent the original depositional surface of the coastal marsh. Two samples of seeds from different trenches from the peat top of the TLS site resulted in the same age of 2540 BCE (^{14}C ages of 4015 ± 45 and 4020 ± 40 yr BP, respectively, Table 2). This corresponds very well with the Yushan profile, both in terms of the stratigraphy and the age of the marine inundation as dated by OSL (2575 BCE; Table 3). From these two reliable and independent lines of chronological evidence which give a range of 2540–2575 BCE for the central age, we therefore consider that the most likely date of the storm to be ~2560 ± 100 BCE (the range of ±100 years was decided according to the error of radiocarbon dating).

The Liangzhu people abandoned the Yushan site immediately after the storm event. Our compilation of radiocarbon ages of other sites across the south Yangtze coastal plains further demonstrates that the terminal age of the Liangzhu culture was at approximately 2500 BCE (Fig. 5), when the Liangzhu people abandoned their state capital complex (Zhang et al., 2015b; Wang et al., 2017). Thus, the Liangzhu culture ended only decades after the Yushan storm. The subsequent Qianshanyang and Guangfulin cultures both lasted only for ~300 years, much shorter than the Liangzhu culture (Fig. 5).

4.3. Relative sea-level change from 4500 to 1500 BCE

The deposits of saltmarsh and freshwater marsh of layers 7 and 6, respectively imply that relative sea level dropped from −0.78 ± 0.22 m to −1.10 ± 0.25 m during the period from late Hemudu (3945–4170 BCE) to Liangzhu culture (2635–2880 BCE; Table 4; Fig. 6). We further interpolated an indicator of the peat top from the west part of unit T0513, where weak erosion of the peat occurred, and ~30-cm thick peat exists above the Holocene base (Fig. 2B). An original ~40-cm thickness of the peat was estimated using the highest estimation of percentage (30%) of peat compaction with an overburden of 1 m (van Asselen et al., 2011). Thus, the original altitude of the peat top and the relative sea level was estimated to be at 1.16 m and −0.70 ± 0.25 m, respectively (Table 4) when the storm occurred at 2560 ± 100 BCE. The upper tidal flat facies of layer 4 indicates a high relative sea-level stand at ~0.25 ± 0.27 m at 2335–2495 BCE while the saltmarsh sediments of layer 3 indicate the sea level was at ~0.05 ± 0.22 m at 1395–1500 BCE. These data suggest an acceleration in relative sea-level rise during the late stage of Liangzhu culture and a slight drop of the sea level from ~2440 BCE. In addition, a rapid relative sea-level rise also occurred from −1.49 ± 0.25 m to −0.45 ± 0.27 m from 4440–4540 BCE to 4260–4360 BCE, inferred from the basal peat layer 9 and the marine-originated homogenous mud layer 8, respectively (Figs. 2B and 4; Table 4). Similarly, this earlier acceleration of sea-level rise occurred during the cultural interruption period between early to mid-Hemudu and late Hemudu cultures (Fig. 6).

5. Discussion

5.1. Flooding signatures across the south Yangtze coast

From these multiproxy and independent lines of evidence, we speculate that a major coastal storm occurred at ~2560 ± 100 BCE, which not only overwhelmed the Yushan site directly, but was strong enough to erode away ~30-cm thick peat (Fig. 3). This storm was followed by long-lasting marine inundation and the development of a brackish tidal flat owing to relative sea-level rise, which led to human abandonment of the area for ~1000 years until ~1625 BCE (Figs. 4 and 6). The brackish wetland ecosystem was characterised by low primary productivity, bacterial-dominated OC and low terrestrial OC input, probably with limited biomass production, and was unlikely to support significant human populations during the high sea-level stand of 2440–1625 BCE (Fig. 4). Although the wetland had become less saline by the time of the subsequent Shang, Zhou, Tang and Song dynasties (layers 2 and 3), we infer from the geochemical data (especially TOC% and TOC/TN) that primary productivity was far lower than it had been during the Liangzhu period (Fig. 4A).

Comparisons with the data available from previous studies of the south Yangtze coast (Fig. 6; Table 5) reveal the extent of this coastal flooding in response to the accelerated sea-level rise during the later stages of Neolithic culture. As expected, a strong saline event occurred at ~2540 BCE at sites within the Yaojiang plain (cf. at TSL; Zheng et al., 2012), but it is also clearly seen 140 km west (at KHQ; ZPICRA, 2004, Fig. 6). A slight increase in salinity (reflected by increase in the abundance of saline Chenopodiaceae) was also seen at the Liangzhu site close to the state capital (Table 5). The marine flooding likely did not extend across the Taihu Plain, which also had some protection from substantial chenier ridges to the east (Fig. 1), but there is evidence of a salinization event at the same time at sites ZX-1, TMC (Fig. 6) and Guangfulin (Table 5) close to the shoreline. At most other sites, an increase in local water level was reported at the end of the Liangzhu period (Table 5), implying inland flooding from storm rainfall or waterlogging due to sea-level rise.

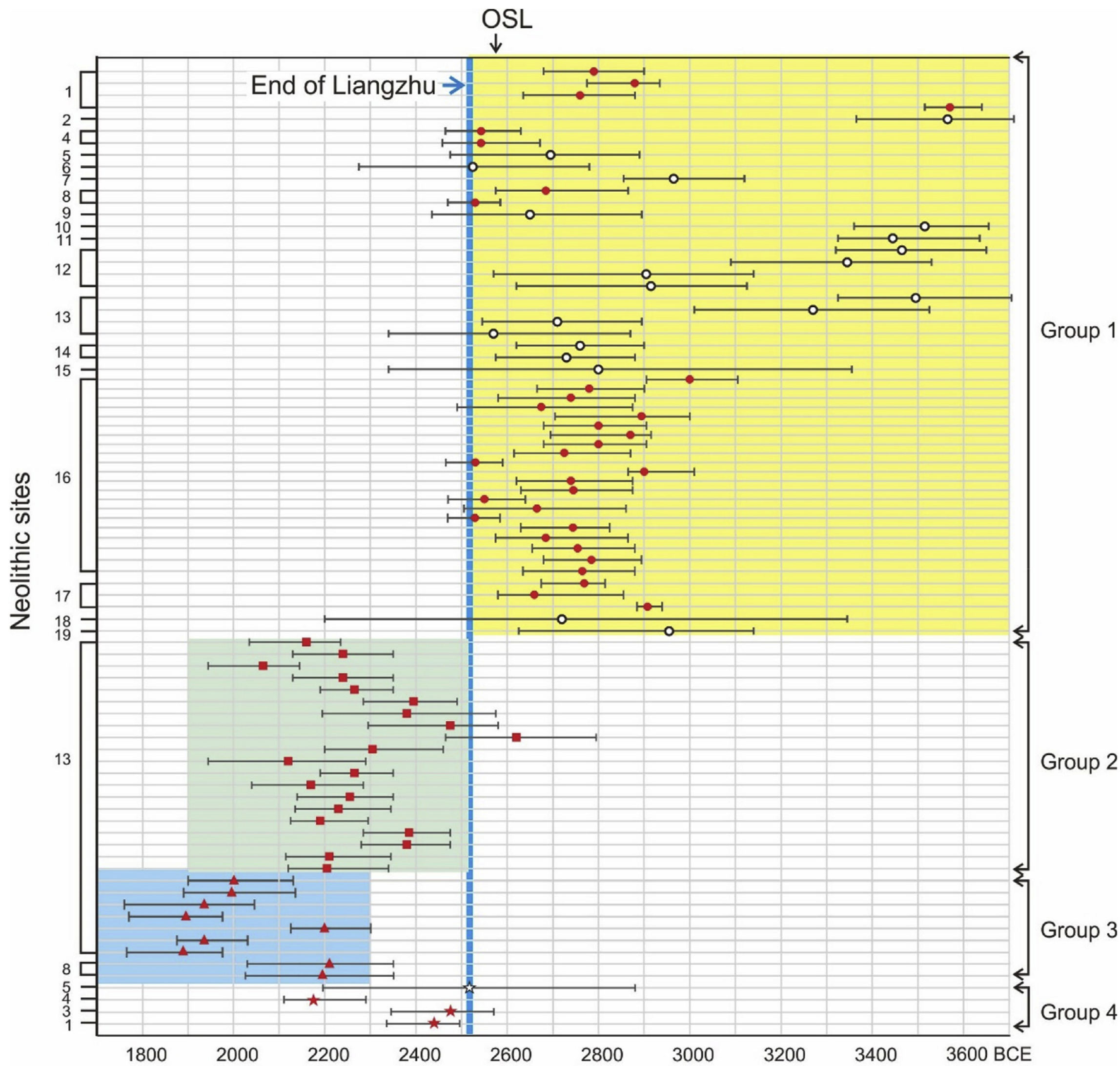

Fig. 5. Time span of the Liangzhu (Group 1), Qianshanyang (Group 2), Guangfulin (Group 3) cultures and post-Liangzhu natural deposits in Yaojiang plain (Group 4). Note the end of the Liangzhu culture is around 2500 BCE. Also indicated is the OSL age of the storm sand at the top of the Liangzhu cultural layer (boundary of layer 5/6a; Fig. 3). Site number ordered by distance from the Yushan site (Fig. 1; Table S1). Samples dated by AMS ^{14}C are indicated in red. Others were dated by the radiometric method. (For interpretation of the references to colour in this figure legend, the reader is referred to the Web version of this article.)

5.2. Causes of the mid-Holocene coastal flooding

Our reconstruction of relative sea level demonstrated a rapid rise (~0.95 m in ~120 years; Table 4) at the final stage of the Liangzhu culture (Fig. 6). The amplitude of this rise could be slightly overestimated because of the uncertainty in the height of the top of the peat and the underestimation of its compaction. We also did not consider the enlargement of the tidal range because previous simulations demonstrated little change in the amplitude of the M_2 tide in the south east Hangzhou Bay during the middle to late Holocene (Uehara et al., 2002). As previous studies further suggest no major deposition or shoreline advance during the middle Holocene along the Hangzhou Bay (Yan et al., 1989; Gao and Collins, 2014; Zhang et al., 2015a), we infer no significant change in tidal levels after the Yushan storm ~4500 years ago.

This accelerated relative sea-level rise is consistent with sea level records from other regions around the world, and adds to evidence that this rise may reflect a global signal, rather than resulting from local processes. For example, on the coast of Peninsular Malaysia, the relative sea level dropped slightly from 3500 to 2500 BCE and then rose suddenly by ~1–3 m from ~2500 to 2100 BCE (Tjia, 1996; Horton et al., 2005). Rapid relative sea level rise between 2650 and 2350 BCE was also reported from the coast of north-eastern Brazil (~1 m; Suguio et al., 2013) and the northern Gulf of Mexico (Balsillie and Donoghue, 2011). In the mid-Pacific Ocean, microatolls record a relative sea level rise beginning at ~2500 BCE, following slightly declining or stable levels over the previous ~1500 years (Woodroffe et al., 2012). The eustatic sea level curve reconstructed from Red Sea corals shows that sea level began to rise at ~2300 BCE, following stable or declining levels over the previous ~900 years (Siddall et al., 2003). These data imply a small but significant acceleration in global sea level rise in the middle of the third millennium BCE.

In addition, Meltzner et al. (2017) reported a half-meter sea level excursion on centennial timescales between 6850 and 6500 cal yr BP from the microatolls of the Sunda Shelf, which indicates that the regional relative sea-level change could be a highly fluctuating pattern along the west coast of the Pacific Ocean. We infer that the

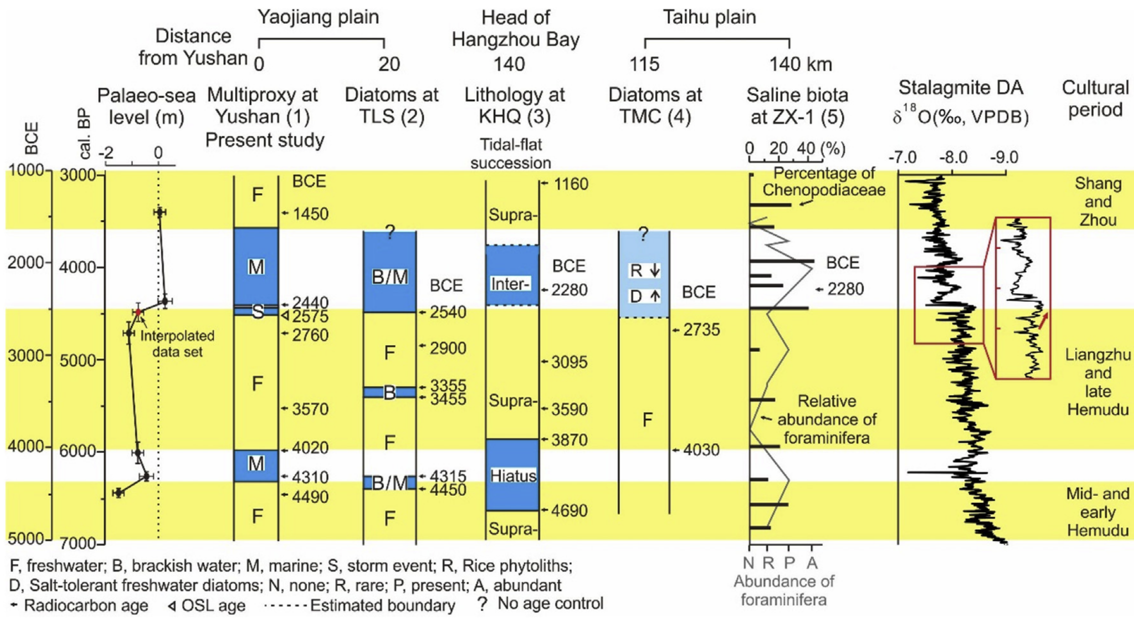

Fig. 6. Comparison of the relative sea-level change and regional marine flooding records on the south Yangtze coast from the Yaojiang and Taihu plains and the head of Hangzhou Bay. In the sea-level curve, calibrated radiocarbon ages are presented with error bars of 2σ; horizontal error bars represent the indicative meaning (range of relative sea level) of each sea-level indicator. The interpolated data point is calculated from the data set derived from the estimated storm age and original peat top (Table 4; see text for details). Sediment profiles are numbered as in Fig. S2 (with increasing distance from Yushan); data sources are given in Tables 4 and S2. The oxygen isotopic record ($\delta^{18}O$) of stalagmite DA from Dongge Cave (the cave location is marked in Fig. 1A; Wang et al., 2005) denotes a short period of strengthening, yet variable, Asian summer monsoon linked to the warming climate (denoted by the red arrow) during the latter stages of the Liangzhu culture. (For interpretation of the references to colour in this figure legend, the reader is referred to the Web version of this article.)

rapid rise of relative sea level at Yushan ~4500 years ago, together with the earlier rise ~6300 years ago (Fig. 6) have similarity with the records in the microatolls of the Sunda Shelf. Furthermore, the record of the Asian summer monsoon shows a small peak in activity from ~2600 to 2450 BCE (Fig. 6; Wang et al., 2005). A comparison of values between the Dongge Cave $\delta^{18}O$, a proxy for the relative strength of the Asian summer monsoon, and atmospheric $\Delta^{14}C$, a proxy for solar activity, revealed that the monsoon peak coincided with the peak in solar irradiance from ~2600 to 2400 BCE (Stuiver, 1998; Wang et al., 2005). From these data, we infer that this small monsoon intensity peak was driven by increasing solar activity and hence was a climate-warming event on a centennial timescale. Therefore, we suggest that accelerated global sea-level rise occurred against a backdrop of climate warming during the late stage of the Liangzhu culture.

Previous studies suggested that a key feature of accelerated rising sea level is that the return periods of flood events decrease as the sea level increases (Sweet et al., 2014; Tessler et al., 2015). We thus suggest that the catastrophic storm at Yushan marked the beginning of a period of frequent flooding across the Yangtze coast, likely including other major coastal and inland flooding events, as supported by evidence of flood deposits in the coastal lowland of Hangzhou Bay and increasing freshwater levels across the Taihu Plain (Fig. 6; Table 5).

5.3. *Impacts of the coastal flooding on the Liangzhu human society*

We argue that perhaps only over a few decades, the combined effect of a series of extreme events and flooding, such as the Yushan inundation, could have overwhelmed even a politically advanced, technologically capable and well-organised prehistoric society such as the Liangzhu. Frequent extreme events and flooding would have had profound impacts, both immediate and longer-term. The coastal storm recorded at Yushan at 2560 BCE and associated flooding (including inland river flooding from storm rainfall) would have destroyed settlements and infrastructure across the region, as seen in the archaeological record at Yushan (Fig. 3). In the Yaojiang Plain, the immediate aftermath of marine flooding would have killed freshwater wetland plant communities that could not tolerate higher salinity and thus ended rice cultivation (Zheng et al., 2012); low net biomass production under marine/brackish conditions (Fig. 4A) would be unlikely to support significant human populations. At the head of Hangzhou Bay, coastal flooding also inundated the late-Liangzhu rice paddies such as at Maoshan (~30 km away from the Mojiaoshan, Fig. 1), notwithstanding it was designed with artificial ditches to facilitate water management (Zhuang et al., 2014). The political centre of Mojiaoshan was not only threatened directly by the salt intrusion and frequent flooding (Liu and Chen, 2012; Zhuang et al., 2014, Table 4), but also could have learned lessons from the flooding of inundated sites in the Yaojiang Plain.

Furthermore, although societal and demographic recovery from a single extreme event could have happened after the Yushan storm (e.g. during freshening seen in the upper section of layer 5; Fig. 4A), frequent flooding would have made this much more difficult, for example by ruining stored rice seeds or from persistent and widespread crop failure (Stone, 2009). This would quickly result in a shortage of surplus production needed to support the political centre, and the large number of artisanal workers not employed in food production, such as jade workers (Liu and Chen, 2012). It is possible that the Liangzhu ruling political elite could have moved the state capital away from the coastal lowland as an adaptive strategy to mitigate the impacts of rising sea level and increasing flooding, potentially explaining the appearance of the subsequent, but less organised and less developed (yet culturally related), Qianshanyang culture. Owing to its profound impacts on the landscape and people, this period of flooding, including the Yushan storm at 2560 BCE, may even have contributed to the ancient oral flood traditions in the Lower Yangtze, forming the cultural setting for the legend of China's Great Flood more than 4000 years ago (Lewis, 2006).

6. Conclusions

From the sedimentary record at the Yushan archaeological site, and combined evidence from other sites in the south Yangtze coastal plain, we conclude that major coastal flooding occurred at the late stage of the Liangzhu culture. This flooding was characterized by extreme events, and was caused by short-term but significant acceleration in sea-level rise, which was possibly linked to a climate warming event on a centennial timescale. We suggest that the frequent extreme events and catastrophic flooding during warming climate phases are controlling factors in explaining Neolithic cultural transitions in the middle Holocene in the Yangtze coastal lowland, including the sudden and perplexing demise of the technologically advanced Liangzhu culture. Our finding of this catastrophic coastal flooding at the middle of third millennium BCE provides an analogue for flood risk, owing to the predicted high rate of sea level rise at the end of 21st century (Nerem et al., 2018) and urgently calls for mitigation strategies to be put in place to protect vulnerable coastal populations worldwide against a similar scenario of abrupt sea level rise in the near future.

Acknowledgements

This study was supported by the National Natural Science Foundation of China (Grant No. 41576042). We are grateful to two anonymous reviewers for their helpful comments.

Appendix A. Supplementary data

Supplementary data related to this article can be found at https://doi.org/10.1016/j.quascirev.2018.03.001.

References

Atahan, P., Itzstein-Davey, F., Taylor, D., Dodson, J., Qin, J., Zheng, H., Brooks, A., 2008. Holocene-aged sedimentary records of environmental changes and early agriculture in the lower Yangtze, China. Quat. Sci. Rev. 27, 556–570. https://doi.org/10.1016/j.quascirev.2007.11.003.

Balsillie, J.H., Donoghue, J.F., 2011. Northern Gulf of Mexico sea-level history for the past 20,000 years. In: Buster, N.A., Holmes, C.W. (Eds.), Gulf of Mexico Origin, Waters, and Biota, vol. 3. Texas A&M University Press, Texas, pp. 53–72. Geology.

Bøtter-Jensen, L., Andersen, C.E., Duller, G.A.T., Murray, A.S., 2003. Developments in radiation, stimulation and observation facilities in luminescence measurements. Radiat. Meas. 37, 535–541. https://doi.org/10.1016/S1350-4487(03)00020-9.

Chen, J., 2002. The Neolithic Culture and Environment in the Yangtze Delta Plain. PhD. Thesis. East China Normal University, Shanghai, p. 109 (in Chinese).

Chen, J.Y., Zhu, H.F., Dong, Y.F., Sun, J.M., 1985. Development of the Changjiang estuary and its submerged delta. Continent. Shelf Res. 4, 47–56.

Chen, Z., Wang, Z., Schneiderman, J., Cai, Y., 2005. Holocene climate fluctuations on millennium scale in the Yangtze delta of eastern China: implications and response. Holocene 15, 917–926.

Duller, G.A.T., 2008. Single-grain optical dating of Quaternary sediments: why aliquot size matters in luminescence dating. Boreas 37, 589–612. https://doi.org/10.1111/j.1502-3885.2008.00051.x.

Durcan, J.A., King, G.E., Duller, G.A.T., 2015. DRAC: dose rate and age calculation for trapped charge dating. Quat. Geochronol. 28, 54–61.

Gao, S., Collins, M.B., 2014. Holocene sedimentary systems on continental shelves. Mar. Geol. 352, 268–294.

Giosan, L., Syvitski, J., Constantinescu, S., Day, J., 2014. Climate change: protect the world's deltas. Nature 516, 31–33.

He, C.Q., Song, Z.C., Zhu, Y.H., 2009. Dinoflagellate Fossil of China. Science Press, Beijing (in Chinese).

Hori, K., Saito, Y., Zhao, Q., Cheng, X., Wang, P., Sato, Y., Li, C., 2001. Sedimentary facies of the tide-dominated paleo-Changjiang (Yangtze) estuary during the last transgression. Mar. Geol. 177, 331–351.

Horton, B.P., Gibbard, P.L., Milne, G.M., Morley, R.J., Purintavaragul, C., Stargardt, J.M., 2005. Holocene sea levels and palaeoenvironments, Malay-Thai Peninsula, southeast Asia. Holocene 15, 1199–1213.

Innes, J.B., Zong, Y., Wang, Z., Chen, Z., 2014. Climatic and palaeoecological changes during the mid- to Late Holocene transition in eastern China: high-resolution pollen and non-pollen palynomorph analysis at Pingwang, Yangtze coastal lowlands. Quat. Sci. Rev. 99, 164–175. https://doi.org/10.1016/j.quascirev.2014.06.013.

Itzstein-Davey, F., Atahan, P., Dodson, J., Taylor, D., Zheng, H., 2007. Environmental and cultural changes during the terminal Neolithic: Qingpu, Yangtze delta, eastern China. Holocene 17, 875–887. https://doi.org/10.1016/j.quascirev.2007.11.003.

Kopp, R.E., Kemp, A.C., Bittermann, K., Horton, B.P., Donnelly, J.P., Gehrels, W.R., Hay, C.C., Mitrovica, J.X., Morrow, E.D., Rahmstorf, S., 2016. Temperature-driven global sea-level variability in the Common Era. Proc. Natl. Acad. Sci. U.S.A. 113, E1434–E1441. https://doi.org/10.1073/pnas.1517056113.

Lamb, A.L., Wilson, G.P., Leng, M.J., 2006. A review of coastal palaeoclimate and relative sea-level reconstructions using $\delta^{13}C$ and C/N ratios in organic material. Earth Sci. Rev. 75, 29–57. https://doi.org/10.1016/j.earscirev.2005.10.003.

Lawler, A., 2009. Beyond the Yellow River: how China became China. Science 325, 930–935. https://doi.org/10.1126/science.325_930.

Lewis, M.E., 2006. The Flood Myths of Early China. State University of New York Press, New York, p. 256.

Li, C., Wang, P., Sun, H., Zhang, J., Fan, D., Deng, B., 2002. Late Quaternary incised-valley fill of the Yangtze delta (China): its stratigraphic framework and evolution. Sediment. Geol. 152, 133–158.

Li, Y., Wu, J., Hou, S., Shi, C., Mo, D., Liu, B., Zhou, L., 2010. Palaeoecological records of environmental change and cultural development from the Liangzhu and Qujialing archaeological sites in the middle and lower reaches of the Yangtze River. Quat. Int. 227, 29–37. https://doi.org/10.1016/j.quaint.2010.05.015.

Liu, L., Chen, X., 2012. The Archaeology of China: from the Late Paleolithic to the Early Bronze Age (Cambridge World Archaeology). Cambridge University Press, Cambridge, p. 475.

Liu, C., Sui, J., He, Y., Hirshfield, F., 2013. Changes in runoff and sediment load from major Chinese rivers to the Pacific Ocean over the period 1955–2010. Int. J. Sediment Res. 28, 486–495.

Liu, B., Wang, N., Chen, M., Wu, X., Mo, D., Liu, J., Xu, S., Zhuang, Y., 2017. Earliest hydraulic enterprise in China, 5,100 years ago. Proc. Natl. Acad. Sci. Unit. States Am. 114, 13637–13642.

Mao, L.M., Wang, W.M., Shu, J.W., Yang, X.L., 2011. Holocene Spores and Microscopic Algae from the Yangtze Delta, East China Acta Palaeontologica Sinica, vol. 50, pp. 154–165 (in Chinese, with English abstract).

Meltzner, A.J., Switzer, A.D., Horton, B.P., Ashe, E., Qiu, Q., Hill, D.F., Bradley, S.L., Kopp, R.E., Hill, E.M., Majewski, J.M., Natawidjaja, D.H., Suwargadi, B.W., 2017. Half-metre sea-level fluctuations on centennial timescales from mid-Holocene corals of Southeast Asia. Nat. Commun. 8, 14387,. https://doi.org/10.1038/ncomms14387.

Moore, P.D., Webb, J.A., Collinson, M.E., 1990. Pollen Analysis. Blackwell Scientific Publications, Oxford.

Nerem, R.S., Beckley, B.D., Fasullo, J.T., Hamlington, B.D., Masters, D., Mitchum, G.T., 2018. Climate-change-driven accelerated sea-level rise detected in the altimeter era. Proc. Natl. Acad. Sci. U.S.A. https://doi.org/10.1073/pnas.1717312115.

Nicholls, R.J., Cazenave, A., 2010. Sea-level rise and its impact on coastal zones. Science 328, 1517–1520. https://doi.org/10.1126/science.1185782.

Qin, L., 2013. The Liangzhu culture. In: Underhill, A.P. (Ed.), A Companion to Chinese Archaeology. Wiley-Blackwell, pp. 574–598.

Qin, J., Taylor, D., Atahan, P., Zhang, X., Wu, G., Dodson, J., Zheng, H., Itzstein-Davey, F., 2011. Neolithic agriculture, freshwater resources and rapid environmental changes on the lower Yangtze, China. Quat. Res. (Duluth) 75, 55–65. https://doi.org/10.1016/j.yqres.2010.07.014.

Renberg, I., 1990. A procedure for preparing large sets of diatom slides from sediment cores. J. Paleolimnol. 4, 87–90.

Ryves, D.B., Clarke, A.L., Appleby, P.G., Amsinck, S.L., Jeppesen, E., Landkildehus, F., Anderson, N.J., 2004. Reconstructing the salinity and environment of the Limfjord and Vejlerne Nature Reserve, Denmark, using a diatom model for brackish lakes and fjords. Can. J. Fish. Aquat. Sci. 61, 1988–2006. https://doi.org/10.1139/F04-127.

Shanghai Museum, 2002. The excavated report on the Neolithic site GUANG FU LIN, Songjiang, Shanghai during 1999-2000. KAO GU 10, 31–48 (in Chinese).

Shennan, I., Long, A.J., Horton, B.P., 2015. Handbook of Sea-level Research. John Wiley &Sons, Ltd.

Siddall, M., Rohling, E.J., Almogi-Labin, A., Hemleben, Ch, Meischner, D., Schmelzer, I., Smeed, D.A., 2003. Sea-level fluctuations during the last glacial cycle. Nature 423, 853–858. https://doi.org/10.1038/nature01690.

Stanley, D.J., Chen, Z., Song, J., 1999. Inundation, sea-level rise and transition from Neolithic to Bronze age cultures, Yangtze delta, China. Geoarchaeology 14, 15–26.

Stone, R., 2009. One year after a devastating cyclone, a bitter harvest. Science 324, 715. https://doi.org/10.1126/science.324_715.

Stuiver, M., 1998. INTCAL 98 radiocarbon age calibration, 24,000-0 cal BP. Radiocarbon 40, 1041–1083.

Stuiver, M., Reimer, P.J., Reimer, R., 2015. CALIB: Radiocarbon Calibration. http://calib.qub.ac.uk/calib/(September2015).

Suguio, K., Barreto, A.M.F., de Oliveira, P.E., Bezerra, F.H.R., Vilela, M.C.S.H., 2013. Indicators of Holocene sea level changes along the coast of the states of Pernambuco and Paraíba. Brazil. Geologia USP 13, 141–152. https://doi.org/10.5327/Z1519-874X201300040008.

Sweet, W., Park, J., Marra, J., Zervas, C., Gill, S., 2014. Sea Level Rise and Nuisance Flood Frequency Changes Around the United States. NOAA Technical Report NOS CO-OPS 073, p. 58.
Syvitski, J.P.M., Kettner, A.J., Overeem, I., Hutton, E.W.H., Hannon, M.T., Brakenridge, G.R., Day, J., Vorosmarty, C., Saito, Y., Giosan, L., Nicholls, R.J., 2009. Sinking deltas due to human activities. Nat. Geosci. 2, 681–686.
Tang, L.Y., Mao, L.M., Li, X.M., 2013. Palaeoecological and palaeoenvironmental significance of some important spores and micro-algae in Quaternary deposits. Chin. Sci. Bull. 58, 3125–3139.
Tessler, Z.D., Vörösmarty, C.J., Grossberg, M., Gladkova, I., Aizenman, H., Syvitski, J.P.M., Foufoula-Georgiou, E., 2015. Profiling risk and sustainability in coastal deltas of the world. Science 349, 638–643. https://doi.org/10.1126/science.aab3574.
Tjia, H.D., 1996. Sea-level changes in the tectonically stable Malay-Thai Peninsular. Quat. Int. 31, 95–101.
Uehara, K., Saito, Y., Hori, K., 2002. Paleotidal regime in the Changjiang (Yangtze) estuary, the east China sea, and the Yellow Sea at 6 ka and 10 ka estimated from a numerical model. Mar. Geol. 183, 179–192.
van Asselen, S., Karssenberg, D., Stouthamer, E., 2011. Contribution of peat compaction to relative sea-level rise within Holocene deltas. Geophysics Research Letters 38, L24401. https://doi.org/10.1029/2011GL049835.
Wang, X., Mo, D., Li, C., Yu, S.-Y., Xue, B., Liu, B., Wang, H., Shi, C., 2017. Environmental changes and human activities at a fortified site of the Liangzhu culture in eastern China: evidence from pollen and charcoal records. Quat. Int. 438, 189–197. https://doi.org/10.1016/j.quaint.2017.05.001.
Wang, Y., Cheng, H., Edwards, R.L., He, Y., Kong, X., An, Z., Wu, J., Kelly, M.J., Dykoski, C.A., Li, X., 2005. The Holocene Asian monsoon: links to solar changes and North Atlantic climate. Science 308, 854–857. https://doi.org/10.1126/science.1106296.
Wang, Z., Li, M., Zhang, R., Zhuang, C., Liu, Y., Saito, Y., Xie, J., Zhao, B., 2011. Impacts of human activity on the late-Holocene development of the subaqueous Yangtze delta, China, as shown by magnetic properties and sediment accumulation rates. Holocene 21, 393–407.
Wang, Z., Zhuang, C., Saito, Y., Chen, J., Zhan, Q., Wang, X., 2012. Early mid-Holocene sea-level change and coastal environmental response on the southern Yangtze delta plain, China: implications for the rise of Neolithic culture. Quat. Sci. Rev. 35, 51–62. https://doi.org/10.1016/j.quascirev.2012.01.005.
Wang, Z., Zhan, Q., Long, H., Saito, Y., Gao, X., Wu, X., Li, L., Zhao, Y., 2013. Early to mid-Holocene rapid sea-level rise and coastal response on the southern Yangtze delta plain, China. J. Quat. Sci. 28, 659–672.
Woodroffe, C.D., McGregor, H.V., Lambeck, K., Smithers, S.G., Fink, D., 2012. Mid-Pacific microatolls record sea-level stability over the past 5000 yr. Geology 40, 951–954. https://doi.org/10.1130/G33344.1.
Woodruff, J.D., Irish, J.L., Camargo, S.J., 2013. Coastal flooding by tropical cyclones and sea-level rise. Nature 504, 44–52. https://doi.org/10.1038/nature12855.
Yan, Q., Xu, S., Shao, X., 1989. Holocene cheniers in the Yangtze delta, China. Mar. Geol. 90, 337–343.
Zhan, Q., Wang, Z., Xie, Y., Xie, J., He, Z., 2012. Assessing C/N and $\delta^{13}C$ as indicators of Holocene sea level and freshwater discharge changes in the subaqueous Yangtze delta, China. Holocene 22, 697–704.
Zhang, X., Dalrymple, R.W., Yang, S.-Y., Lin, C.-M., Wang, P., 2015a. Provenance of Holocene sediments in the outer part of the paleo-Qiantang River estuary, China. Mar. Geol. 366, 1–15.
Zhang, X., Huang, D., Deng, H., Snape, C., Meredith, W., Zhao, Y., Du, Y., Chen, X., Sun, Y., 2015b. Radiocarbon dating of charcoal from the Bianjiashan site in Hangzhou: new evidence for the lower age limit of the Liangzhu Culture. Quat. Geochronol. 30, 9–17. https://doi.org/10.1016/j.quageo.2015.07.001.
Zhao, X., 1998. Origin of rice paddy cultivation at the Hemudu site. Agricultural Archaeology 1, 131–137 (Scanned by Sui, K.; form. by Leir, G.; transl./ed. by Gordon, B., Wong, E., Craig, A.).
Zheng, Y., Sun, G., Qin, L., Li, C., Wu, X., Chen, X., 2009. Rice fields and modes of rice cultivation between 5000 and 2500 BC in east China. J. Archaeol. Sci. 36, 2609–2616. https://doi.org/10.1016/j.jas.2009.09.026.
Zheng, Y.F., Sun, G.P., Chen, X.G., 2012. Response of rice cultivation to fluctuating sea level during the Mid-Holocene. Chin. Sci. Bull. 57, 370–378. https://doi.org/10.1007/s11434-011-4786-3.
Zhuang, Y., Ding, P., French, C., 2014. Water management and agricultural intensification of rice farming at the late-Neolithic site of Maoshan, Lower Yangtze River, China. Holocene 24, 531–545. https://doi.org/10.1177/0959683614522310.
Zong, Y., Chen, Z., Innes, J.B., Chen, C., Wang, Z., Wang, H., 2007. Fire and flood management of coastal swamp enabled first rice paddy cultivation in east China. Nature 449, 459–462. https://doi.org/10.1038/nature06135.
Zong, Y., Innes, J.B., Wang, Z., Chen, Z., 2011. Mid-Holocene coastal hydrology and salinity changes in the east Taihu area of the lower Yangtze wetlands, China. Quat. Res. (Duluth) 76, 69–82. https://doi.org/10.1016/j.yqres.2011.03.005.
Zong, Y., Innes, J.B., Wang, Z., Chen, Z., 2012. Environmental change and Neolithic settlement movement in the lower Yangtze wetlands of China. Holocene 22, 659–673. https://doi.org/10.1177/0959683611414933.
ZPICRA, 2004. KUA HU QIAO-archaeological Report of Puyang River Valley I. Beijing. WEN WU Press, p. 379 (in Chinese).
ZPICRA, Huzhou Museum, 2014. Qianshanyang: a Report on the Third and Fourth Excavations of the Site. WEN WU Press, Beijing, p. 738 (in Chinese).